NEW SIMULATION AND EXPERIMENTAL METHODOLOGY FOR ANALYZING PULL-IN AND RELEASE IN MEMS SWITCHES

M. Kamon,[1] S. Maity,[1] D. DeReus[2], Z. Zhang[3], S. Cunningham[2], S. Kim[2], J. McKillop[2], A. Morris[2], G. Lorenz[1], L. Daniel[3]
[1]Coventor, Inc. Cambridge, MA, USA [2]Wispry, Irvine, CA, USA [3]MIT, Cambridge MA, USA

ABSTRACT

In this paper we present a new hybrid finite-element/component-modeling approach that can predict the pull-in and release behavior of MEMS switches orders of magnitude faster, and with significantly more behavioral detail, than traditional finite-element or formula-based approaches. The speed and detail allow exploration of the design space, guidance for design-of-experiments, and insight into process variation that was previously infeasible. For instance, the existence of multiple pull-in or release states is very sensitive to device dimensions and is critical to achieving desired performance and yield. Understanding this sensitivity by varying all possible parameters in a traditional finite-element approach could take weeks of simulation. Using the above methodology, the analysis can be done in minutes.

The simulation methodology has been verified by comparing with measured Capacitance-Voltage (CV) relationship and Wyko white light interferometry displacement data for a commercial capacitive switch.

KEYWORDS

MEMS modeling, simulation, pull-in, release, MEMS switch, finite-element, behavioral

INTRODUCTION

Electrostatically actuated MEMS switches have been applied in, for instance, RF [1], digital mirrors [2], and recently logic [3]. Requirements of such switches for low power, reliability and yield have forced designs that cannot be modeled with simplified analytic formulae. For instance, the commercial capacitive switch from wiSpry [4] shown in Figures 1 and 2 is a geometrically complicated, multi-layer long beam fixed rigidly on one end and flexibly on the other. Residual stress produces an initial deflection and small bumps are placed on the electrodes underneath for reliability.

As a result of this complexity, detailed electromechanical analysis tools such as [9] are needed to capture the behavior of these designs. Such tools employ a combination of finite-element and boundary-element analysis and, while very accurate, can take several hours for a single analysis. Varying multiple design parameters to optimize the design or explore sensitivity to process variation can then take days at best. Also because of the long simulation times, voltage sweeps are often done with a coarse set of points, potentially missing subtleties in the response.

Behavioral modeling paradigms [5-8] that offer components with analytic equations for common MEMS building blocks can solve in minutes instead of days but usually cannot be used because the component library is not rich enough to represent the geometric complexity of the design.

This paper presents a hybrid modeling methodology that attains speeds similar to behavioral modeling but with sufficient geometric complexity to model recent MEMS designs. The approach combines high-order finite-elements for mechanics with semi-analytic components for electrostatic forces *including fringing fields*. The methodology has been implemented in the commercial MEMS/IC co-design platform named MEMS+ [10].

The switch shown in Figures 1 and 2 will be created in the MEMS+ platform and simulations will show experimental match to device deformation after pull-in when compared to Wyco displacement data. Simulations will also be compared to CV measurement and shown to accurately predict the structure of the CV curve including effects such as secondary release. The speed of simulation makes the determination of sensitivity to design and process variation possible. To demonstrate, we compare to measured data for varying designed bump heights and process-induced perturbations. Finally, a demonstration of applying advanced algorithms is given and shows the location of hidden instabilities.

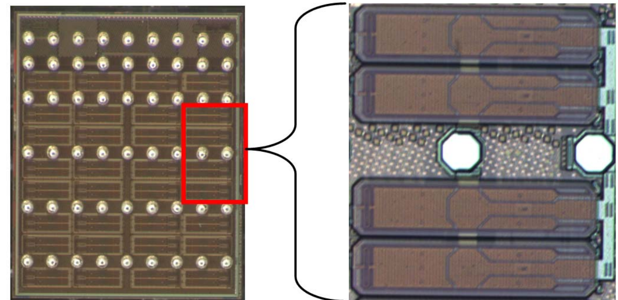

Figure 1. Tunable Capacitor Die and Unit Cell of 4 Tunable Capacitors

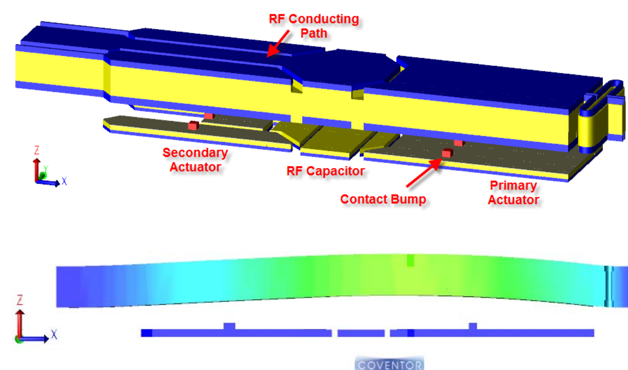

Figure 2: 3D view of MEMS+ switch model and deflection from residual stress. Z dimension is exaggerated 10x for illustration.

MODELING METHODOLOGY

In the original parametric MEMS behavioral modeling methodologies of [5-8], a MEMS device was constructed from building-blocks components such as beams, plates, and electrostatic comb fingers which were represented as symbols in an electrical schematic editor. In MEMS+, the MEMS device is instead constructed in a specialized *3D schematic editor* where the components are rendered as their actual 3D geometry rather than a symbol, and components are connected automatically based on their physical location rather than requiring manual wiring. The details of this platform are described in [11]. A MEMS+ model as shown in Figure 2 may look like a typical feature-based 3D model, but is actually the combined geometry of typically 5 to 100 components. The entire 3D component-based model can be placed as single symbol in an electrical schematic for MEMS-IC co-simulation, or used by itself for fast MEMS analysis as in this paper.

Combining high-order finite-elements for mechanics or fluid damping into this methodology is now practical because the many connections between elements can be determined automatically rather than requiring manual wiring. Also, as part of a specialized 3D environment, the elements can be customized for MEMS to greatly reduce the number of elements needed to represent a design. For instance, in Figure 3a, the multi-layer shell component that is vital for modeling the switch of this paper is a single component, but consists of multiple stacked mixed-interpolation shell elements [12] whose vertically aligned nodes are constrained to move together to reduce the size of the system. Figure 3c illustrates warping of the cross-section of a beam under torsion modeled traditionally with over 1000 finite-element bricks. A single beam component can model the warping of this beam [13] which is vital for beams whose length is not significantly longer than their height, as is common today for inertial sensors etched with deep reactive ion etching (DRIE). Figure 3d shows the parameters to specify a beam of varying-width which can be used, for example, to model a fillet with a single component.

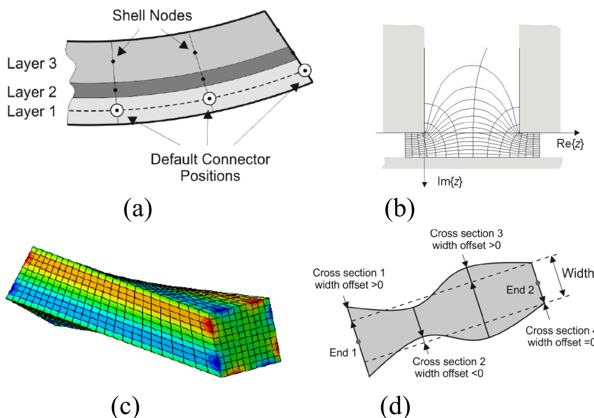

Figure 3: Specialization of Finite-elements for MEMS

Electrostatic forces can be modeled with a simple parallel plate formula only in ideal cases. An analytic formula for more complicated conductor configurations is possible via conformal mapping. Figure 3b shows the electrostatic field pattern for the forces calculated in MEMS+ for the 3 conductor configuration shown. The same technique was used in [14], but has been enhanced to use numerical quadrature to broaden the range of component geometries.

DEVICE AND MODEL

The capacitive switch [4] of Figures 1 and 2 consists of a long, moving beam with a central octagonal RF capacitor. The capacitor plate on the moving beam has an RF conducting path running along the top of one side of the beam. The device is primarily actuated by an electrode underneath the beam on the side opposite the RF conducting path. The remaining area on the other side that is not taken up by the conducting path is used as a secondary actuation electrode. Small bumps shown in red are placed underneath the actuating electrodes to limit the contact and improve reliability. The fabrication process is described in [18].

A full MEMS+ 3D model of the switch is shown in Figure 2. Since it is symmetric about its length, a model of half the design with symmetry boundary conditions is used for simulation. This gives a design with 22 shell components, a J-beam component on the end, and 12 electrode components. The nonlinear system representing this design has only 852 degrees of freedom. The view of the mechanical connectors illustrates the degrees of freedom in Figure 4. Each orange and green ball represents 6 degrees of freedom *(x,y,z,rx,ry,rz)* similar to a finite-element node. Note that some elements have more nodes along their length for locally more accurate computation.

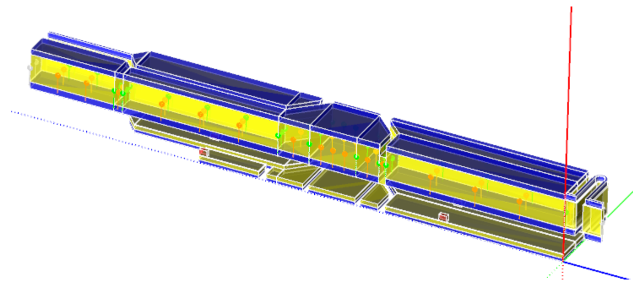

Figure 4: Half-model with symmetry and connectors shown as orange and green balls. Each layer of each component outlined in white.

DEFORMED OPTICAL COMPARISON

Wyco white light interferometry was used first to measure initial deflections which were used to determine residual stress levels. Those residual stress levels, when applied to the model, reproduced the Wyco data. The simulated deformation is shown at the bottom of Figure 2.

Wyco deformation data after 40 V is applied to both primary and secondary actuators is shown in Figure 5 for two different bump heights. The 0.5um bumps successfully keep the beam from collapsing onto the primary actuator while the beam clearly has collapsed on this actuator for 0.1um bumps. Simulation successfully captures this difference as shown by the corresponding simulated shape shown below each measurement in Figure 5.

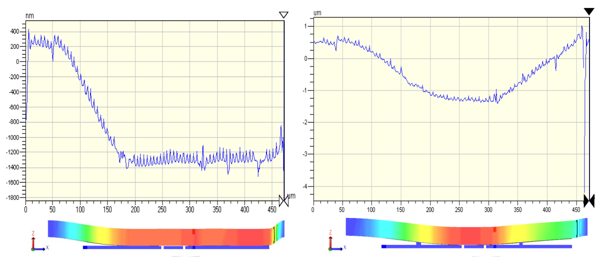

Figure 5: Wyko displacement along length of beam for devices actuated at 40 V. Simulated deflection is shown underneath each measurement.

CV COMPARISON

The contact bumps significantly impact not only the shape of the structure after contact, but also the entire CV relationship while in contact. Figure 6 shows measured CV curves for 3 devices for 0.1um bumps and 3 for 0.5um bumps. The 3 devices are adjacent on the wafer and have different RF capacitor sizes, but identical actuator geometries.

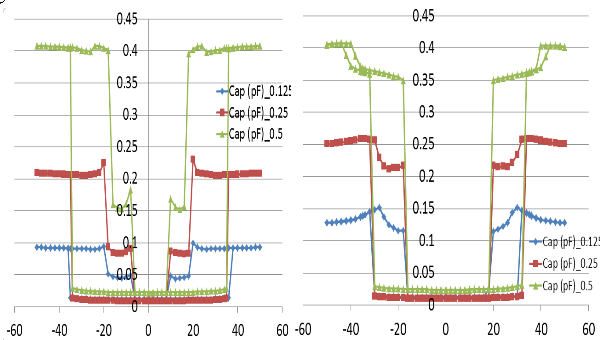

Figure 6: Measured C-V for bump height of 0.1um (left) and 0.5um (right) for adjacent devices with 3 different RF capacitor sizes.

Fully-coupled electromechanical FEM/BEM simulation [9] as implemented in the commercial tool CoventorWare [15] was used to model this behavior as shown in Figure 7. While extremely accurate, each CV curve took hours to compute, which limits design and process variation analysis. Also, the selection of voltage steps required significant user know-how to avoid missing the secondary release instabilities. In contrast, using the MEMS+ model, each CV curve can be computed in less than 5 minutes on a 4-core laptop computer, and with much finer resolution. For instance, in Figure 8, the CV curves for the two nominal bump heights and process variations around those bump heights were computed in about an hour.

The simulated curves clearly capture 3 differences in the measured CV curves between the two bump heights: 1) as the voltage is lowered from pull-in to release, the 0.1um bump devices have a stable capacitance while the 0.5um bump devices decrease significantly. Stability in the region determines the impact of lowering the "on" voltage after pull-in for low power and improved reliability. 2) The 0.1um bump devices have a secondary release voltage while the 0.5um devices release fully at their first instability, and 3) the structure of the 3 CV curves for a given bump height should be similar because the actuator geometries are identical, but the measured 0.5um curves show significant differences in the rate and shape of the drop in capacitance between pull-in and release. This lack of similarity indicates significant sensitivity to process variation. The simulated 0.5um curves show this sensitivity. The region of stable capacitance in Figure 8 for 0.5um bumps is very sensitive to a 10% change in bump height.

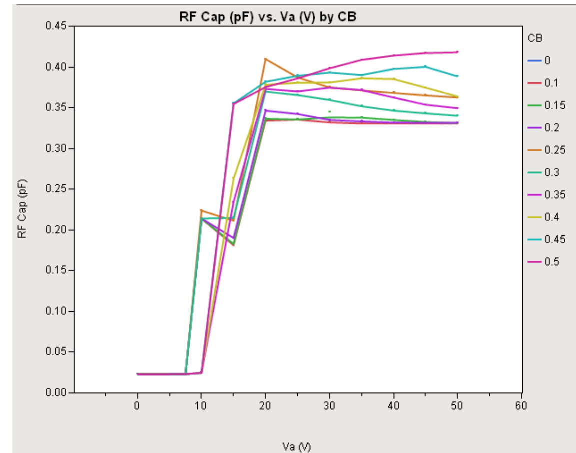

Figure 7: Simulated C-V curve using a coupled FEM/BEM approach.

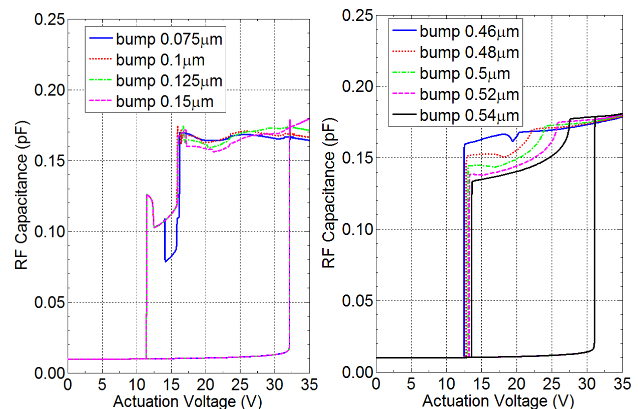

Figure 8: Simulated CV using MEMS+ for 0.1um and 0.5um bump heights

The bump height may not be the sole source of the process sensitivity. Varying multiple critical parameters simultaneously could be done in hours and would give more insight into the true sensitivity.

Varying process parameters does not give direct insight into the origins of other equilibrium states such as secondary release shown here or from partial release due to dielectric charging discussed in [16]. The system of nonlinear, ordinary differential equations defined by the MEMS+ model is available from MATLAB to apply user-defined analyses. In Figure 9, we show applying an arc-length continuation algorithm [17] to the system to find other equilibrium solutions not found with voltage sweeps.

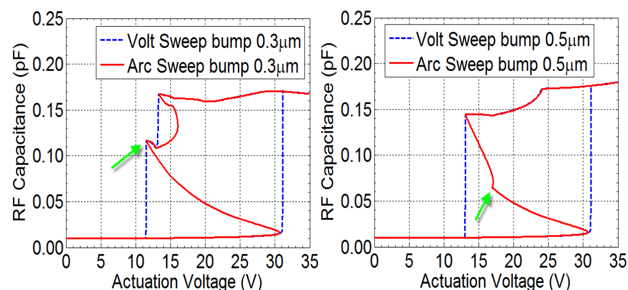

Figure 9: Full equilibrium solutions (red) for 0.3um and 0.5um bump heights overtop voltage sweep solutions (blue). Green arrow marks location of secondary release.

These curves reveal that a solution exists for the secondary release for not only 0.3um bumps, but also for 0.5um bump height. However, for 0.5um bumps the secondary release is larger in voltage and has moved far enough away from the primary release that it will never physically appear with typical process variation but may appear as a result of dielectric charging.

In summary, we have shown a methodology to rapidly compute critical CV characteristics yielding broad insight into switch behavior under design and process variations.

ACKNOWLEDGEMENTS

Wispry would like to acknowledge our partners at IBM Microelectronics in Essex Junction, VT for fabrication of the MEMS capacitive switches.

REFERENCES

[1] S. Pacheco, L. Katehi, and C. Nguyen, "Design of low actuation voltage RF MEMS switch," in *Proc. IEEE Microwave Symp.*, Jun. 2000, pp. 165–168.

[2] L. J. Hornbeck, "Digital light processing and MEMS: an overview," in *Proc. IEEE/LEOS Summer Topic Meetings*, Aug. 1996, pp. 5–7.

[3] F. Chen, H. Kam, D. Markovic, T.-J. K. Liu, V. Stojanovic, and E. Alon, "Integrated circuit design with NEM relays," in *Proc. Intl.Conf. Computer-Aided Design*, Nov. 2008, pp. 750–757.

[4] D. R. DeReus, et al., "Tunable Capacitor Series Shunt Design for Integrated Tunable Wireless Front End Applications," in *IEEE 24th Intl. Conf. Micro Electro Mechanical Systems (MEMS)*, Cancun, MX, 23-27 Jan 2011, pp. 805-808.

[5] G. Lorenz and R. Neul, "Network-type modeling of micromachined sensor systems," in *Proc. Intl. Conf. Modeling Simulation of Microsystems*, Apr. 1998, pp. 233–238.

[6] G. Fedder and Q. Jing, "A hierarchical circuit-level design methodology for microelectromechanical systems," *IEEE Trans. Ciruits and Systems II: Analog and Digital Signal Processing*, vol. 46, no. 10, pp. 1309–1315, Oct. 1999.

[7] J. V. Clark, N. Zhou, and K. S. J. Pister, "MEMS simulation using SUGAR v0.5," in *Proc. Solid-State Sensors Actuators Workshop*. Hilton Head Island, June 1998, pp. 191–196.

[8] M. Maher and H. Lee, "MEMS systems design and verification tools," in *Proc. SPIE Smart Structures Materials*. San Diego, CA, Mar. 1998, pp. 40–48.

[9] X. Cai, et. Al, "A Relaxation/Multipole-Accelerated Scheme for Self-Consistent Electromechanical Analysis of Complex 3-D Microelectromechanical Structure", *Int. Conf. on Computer Aided Design*, Santa Clara, CA 1993.

[10] http://www.coventor.com/products/mems/

[11] G. Schröpfer, G. Lorenz, S. Rouvillois, S. Breit, "Novel 3-D modeling methods for virtual fabrication and EDA compatible design of MEMS via parametric libraries, *Journal of Micromechanics and Microengineering* 20 (2010), 064003

[12] D. Chapelle, and K. J. Bathe. "The mathematical shell model underlying general shell elements," *International Journal for Numerical Methods in Engineering*, 48(2): 289-313, 2000.

[13] Walter D. Pilkey. *Analysis and Design of Elastic Beams: Computational Methods*, John Wiley & Son, Inc, 2002.

[14] G. Lorenz, S. Dickman, "Modeling of electrostatic MEMS components" in *Int. Conf. on Modeling and Simulation of Microsystems, MSM99*, San Juan, 1999.

[15] http://www.coventor.com/products/coventorware/

[16] J. Bielen and J. Stulemeijer, "Efficient electrostatic-mechanical modeling of C-V curves of RF-MEMS switches," in *Proc. EusoSime*, Apr. 2007, pp. 1-6.

[17] Z. Zhang, M. Kamon, L. Daniel "Continuation-Based Pull-In and Lift-Off Simulation for Micro-Electro-Mechanical Design", submitted *J. Microelectromech. Syst.*

[18] A. Stamper et al., "Planar MEMS RF capacitor integration," *Solid-State Sensors, Actuators and Microsystems Conference (TRANSDUCERS),* 2011

CONTACT

*Matt Kamon, 617-497-6880 x227; matt@coventor.com